HHS Public Access

Author manuscript

Eur Biophys J. Author manuscript; available in PMC 2024 July 01.

Published in final edited form as:

Eur Biophys J. 2023 July ; 52(4-5): 311–320. doi:10.1007/s00249-023-01641-4.

A new UltraScan module for the characterization and quantification of analytical buoyant density equilibrium experiments to determine AAV capsid loading

Alexey Savelyev[1], **Emre H. Brookes**[1], **Amy Henrickson**[2], **Borries Demeler**[1,2]

[1]Department of Chemistry and Biochemistry, University of Montana, Missoula, MT, USA

[2]Department of Chemistry and Biochemistry, University of Lethbridge, Lethbridge, AB, Canada

Abstract

A method for characterizing and quantifying peaks formed in an analytical buoyant density equilibrium (ABDE) experiment is presented. An algorithm is derived to calculate the concentration of the density forming gradient material at every point in the cell, provided the rotor speed, temperature, meniscus position, bottom of the cell position, and the loading concentration, molar mass, and partial specific volume of the density gradient-forming material are known. In addition, a new peak fitting algorithm has been developed which allows the user to automatically quantify the peaks formed in terms of density, apparent partial specific volume, and relative abundance. The method is suitable for both ionic and non-ionic density forming materials and can be used with data generated from the UV optical system as well as the AVIV fluorescence optical system. These methods have been programmed in a new UltraScan-III module (*us_abde*). Examples are shown that demonstrate the application of the new module to adeno-associated viral vector preparations and proteins.

Keywords

Analytical ultracentrifugation; Analytical buoyant density equilibrium; AAV quantification and characterization; Peak fitting; UltraScan software

Introduction

Analytical buoyant density gradient equilibrium (ABDE) experiments performed with an analytical ultracentrifuge (AUC) are receiving renewed interest prompted by the need for accurate quantification of capsid loading states of adeno-associated viral vector (AAV)-based gene therapies. ABDE experiments separate solutes present in a mixture based on their buoyant density. The sensitivity of this approach has long been appreciated, and was first demonstrated in the famous experiment performed by Meselson and Stahl (Meselson and Stahl 1958) where buoyant density gradient equilibrium sedimentation was performed

✉Borries Demeler, demeler@gmail.com.

Supplementary Information The online version contains supplementary material available at https://doi.org/10.1007/s00249-023-01641-4.

to prove that DNA replicates semi-conservatively. At equilibrium, Meselson and Stahl were able to separate DNA molecules differentially labeled with two nitrogen isotopes in a cesium chloride density gradient because the relative proportion of the isotopes present in each DNA population imparted a distinct density difference that could be clearly distinguished by ABDE experiments. Preparative buoyant density gradient equilibrium experiments have long been applied to purify supercoiled plasmids (Sambrook et al. 1989) and viral vectors (Wang et al. 2021; Challis et al. 2019; Deng and Oka 2020), and can be used to prepare single walled carbon nanotubes of pure chirality (Green and Hersam 2011). The advantages of ABDE experiments include high resolution, high sensitivity, and very low sample requirements in contrast to sedimentation velocity experiments, which require approximately 20–30 times larger amounts of sample. The potential of ABDE experiments can be exploited in modern AUC instruments, where the accuracy is high because of hardware advances and the possibility of first principle analysis, to permit detailed quantification and reproducible characterization of macromolecular mixtures of molecules with different densities. In an ABDE experiment, the sample is dissolved in a density gradient-forming solvent and spun at high speed (typically 40–60 krpm) until equilibrium is attained. The applied centrifugal force will cause the density gradient-forming material to redistribute and create an exponential distribution of concentration and density inside the AUC cell between the meniscus, where the concentration of the gradient-forming material is lowest, and the bottom of the cell, where it will be the highest. At equilibrium, the gradient no longer changes, and a stable redistribution of the solutes is achieved, which will separate all solutes based on density in near-Gaussian peaks at positions in the density gradient that equal the buoyant density of the corresponding macromolecules. The solutes dissolved in the density gradient-forming solvent are initially uniformly distributed throughout the AUC cell, but will sediment toward the bottom from the meniscus side and float up from the bottom toward the meniscus to collect at a point in the cell where the inverse of their apparent partial specific volume equals the density of the density gradient. The width of the peak will be a function of the steepness of the gradient and the diffusion coefficient of the solute. Another factor of importance to consider in ABDE experiments is the choice of the gradient-forming material. Ionic (CsCl, Cs_2SO_4) and non-ionic (Iodixanol, Nycodenz, Metrizamide) density gradient-forming materials are available. They differ in their applications and the buoyant densities they produce, which will differ especially for charged molecules like DNA. For example, DNA, when measured in a CsCl gradient, will be highly complexed with Cs ions, increasing its apparent density. On the other hand, when measured in Nycodenz, in the absence of significant amounts of metal ions, the charged anionic DNA molecules will be highly hydrated, reducing the DNA's apparent density significantly. Hence, it is important to test the density of a particular biopolymer with a known standard that has similar or identical physico-chemical properties in the selected density gradient material. With particular focus on the need for accurate AAV characterization, we developed new software to better support the accurate classification and quantification of empty, partial and filled AAV capsids. In this context, the classification of the peaks formed at equilibrium is a question of the peak density at the center of the peak, while the quantification is a question of peak volume. Algorithms for both tasks are presented, and a guide to the new '*us_abde*' module in UltraScan-III (Demeler and Gorbet 2016; Demeler et al. 2022) is provided.

Methods and results

Theory

Peak classification—ABDE experiments separate solutes based on their density. Molecules with the same buoyant density will collect at the same position in the cell, regardless of their shape or molar mass. For example, a DNA molecule will have the same density regardless of sequence or sequence length (as long as the base composition is similar). A 20 base pair (bp) double-stranded DNA fragment will have the same density as a 3,000 bp plasmid, and therefore equilibrate at the same radial position in the density gradient. However, the shorter DNA fragment will have a faster diffusion and will therefore form a broader peak. In this section, we describe how the density of the peak position can be determined. When the rotor is accelerated, the density gradient-forming material will begin to sediment and after some time, equilibrate with sedimentation and diffusion transport balancing out. At this point, the density gradient is established, and the concentration distribution $C(r)$ of the density gradient material will follow an exponential form, given by Eq. 1:

$$C(r) = C_0 \exp\left[\frac{M\omega^2(1-\bar{v}\rho)(r^2 - r_m^2)}{2RT}\right] \tag{1}$$

where r is the distance from the rotor center in cm, M is the molecular weight of the gradient-forming material, C_0 is the reference concentration of the gradient-forming material, ω is the angular velocity of the rotor, and r_m is the reference position, typically the meniscus. The total mass loaded is equal to the loading concentration times the volume. Provided the cell does not leak, the total mass remains constant throughout the experiment and the integral from meniscus to bottom over the entire sector will be equal to the amount loaded:

$$C_{\text{total}} = l\frac{\alpha}{360}2\pi\int_{r_m}^{r_b} rC(r)dr = C_{\text{loading}}\frac{\alpha}{360}\pi l(r_b^2 - r_m^2) \tag{2}$$

where l is the path length of the cell (typically1.2 cm or 0.3 cm), r_b the bottom of the cell and r_m the meniscus, and α is 2.5 degrees, referring to the angular width of the sector of a standard Epon-charcoal 2-channel centerpiece. At equilibrium, we can integrate over the entire cell and equate the integral to the total mass, which is equal to the integral from the meniscus to the bottom of the cell as given by Eq. 2, multiplied by the volume increment:

$$\begin{aligned} &l\frac{\alpha}{360}2\pi\int_{r_m}^{r_b} rC(r)dr \\ &= C_0(r_m)l\frac{\alpha}{360}2\pi\int_{r_m}^{r_b} r\exp\left[\frac{M\omega^2(1-\bar{v}\rho)(r^2 - r_m^2)}{2RT}\right]dr \end{aligned} \tag{3}$$

To obtain C_0, we equate both equations and the path length and arc length cancel:

$$C_{loading}\left(r_b^2 - r_m^2\right) = 2C_0(r_m)\int_{r_m}^{r_b} r\,\exp\left[\frac{M\omega^2\left(1-\bar{v}\rho\right)\left(r^2-r_m^2\right)}{2RT}\right]dr \tag{4}$$

Rearranging yields an equation for the initial concentration:

$$C_0(r_m) = C_{loading}\frac{1}{2}\left(r_b^2 - r_m^2\right)\left[\int_{r_m}^{r_b} r\,\exp\left[\frac{M\omega^2\left(1-\bar{v}\rho\right)\left(r^2-r_m^2\right)}{2RT}\right]dr\right]^{-1} \tag{5}$$

substituting:

$$\begin{aligned} k_1 &= \frac{M\omega^2}{2RT}\left(1-\bar{v}\rho\right) \\ k_2 &= C_{loading}\frac{1}{2}\left(r_b^2 - r_m^2\right) \end{aligned} \tag{6}$$

we obtain:

$$C_0(r_m) = k_2\left[\int_{r_m}^{r_b} r\,\exp\left[k_1\left(r^2 - r_m^2\right)\right]dr\right]^{-1} \tag{7}$$

$$\int re^{k_1\left(r^2-r_m^2\right)}dr = e^{-k_1 r_m^2}\int re^{k_1 r^2}dr = e^{-k_1 r_m^2}\frac{e^{k_1 r^2}}{2k_1} + C \tag{8}$$

$$\begin{aligned} C_0(r_m) &= k_2\left[\int_{r_m}^{r_b} r\,\exp\left[k_1\left(r^2 - r_m^2\right)\right]dr\right]^{-1} \\ &= k_2\left[e^{-k_1 r_m^2}\frac{1}{2k_1}\left(e^{k_1 r_b^2} - e^{k_1 r_m^2}\right)\right]^{-1} \\ &= k_2\left[\frac{1}{2k_1}\left(e^{k_1\left(r_b^2 - r_m^2\right)} - 1\right)\right]^{-1} \\ &= k_2\left[\frac{2k_1}{e^{k_1\left(r_b^2 - r_m^2\right)} - 1}\right] \\ &= \frac{2k_1k_2}{e^{k_1\left(r_b^2 - r_m^2\right)} - 1} \end{aligned} \tag{9}$$

and therefore:

$$
\begin{aligned}
C(r) &= C_0(r_m)\exp\left[\frac{M\omega^2\left(1-\bar{v}\rho\right)\left(r^2-r_m^2\right)}{2RT}\right] \\
&= C_0(r_m)e^{k_1\left(r^2-r_m^2\right)} \\
&= \frac{2k_1k_2}{e^{k_1(r_b^2-r_m^2)}-1}e^{k_1(r^2-r_m^2)} \\
&= 2k_1k_2\frac{e^{k_1(r^2-r_m^2)}}{e^{k_1(r_b^2-r_m^2)}-1}
\end{aligned}
\tag{10}
$$

and substituting Eq. 7, we obtain:

$$
C(r) = C_{\text{loading}}\left(r_{\text{b}}^2-r_{\text{m}}^2\right)\frac{M\omega^2}{2RT}\left(1-\bar{v}\rho\right)\frac{e^{\frac{M\omega^2}{2RT}(1-\bar{v}\rho)(r_{\text{b}}^2-r_{\text{m}}^2)}}{e^{\frac{M\omega^2}{2RT}(1-\bar{v}\rho)(r_{\text{b}}^2-r_{\text{m}}^2)}-1} \tag{11}
$$

The loading concentration is relative to water, which has a density of 1 mg/ml, so when this value is set to 1, the result is the gradient-forming material's concentration relative to the loading concentration. With Eq. 11, it is now possible to determine the concentration of the gradient material at each position r in the AUC cell, provided the following parameters are accurately known: 1. meniscus position; 2. bottom of the cell position; 3. the loading concentration of the gradient-forming material; 4. the molar mass of the gradient-forming material; 5. the partial specific volume of the gradient-forming material; 6. the rotor speed; 7. the temperature of the experiment. Some of these parameters are provided by the instrument (rotor speed, temperature), the molar mass of the gradient material is available from the manufacturer. The bottom of the cell position is subject to rotor stretch, which is speed dependent. Since the bottom position of the cell is often not identifiable from the scan data, a prediction algorithm has been programmed in UltraScan which takes into account the rotor stretch profile, the rotor speed, and the centerpiece geometry. The rotor stretch calibration routine in UltraScan is discussed in (Stoutjesdyk et al. 2020), and is incorporated into the new algorithm. The loading concentration of the gradient-forming material is best determined with a refractometer, especially when the stock solution of the gradient-forming material is diluted by adding an aliquot of the aqueous analyte solution. A refractometer will use just a few microliters of the diluted sample and provide a highly accurate refractive index. The refractive index is directly proportional to the concentration of the gradient-forming material. The last parameter required for a solution of Eq. 11 is the partial specific volume of the gradient-forming material, its measurement is discussed below. The automatic peak fitting algorithm, described below, will identify the radial position of the peak center, which can then be entered into Eq. 11 to determine the concentration of the gradient-forming material at this position. In the next step, the concentration of the gradient-forming material is converted to a density value, obtained from a calibrated reference curve (see reference calibration example below). Once the density of the gradient-forming material is determined, the apparent partial specific volume of an analyte at any peak position is simply the inverse of the density at that point.

Peak fitting algorithm—ABDE experiments generate characteristic peaks of analytes as a result of the underlying density gradient. Hence, in order to improve automated peak identification, a new peak fitting algorithm was developed, and implemented in the '*us_abde*' module of UltraScan (Demeler and Gorbet 2016). Any openAUC dataset (Cölfen et al. 2010) classified as type '*Buoyancy*' must be edited in UltraScan to define the meniscus position and the data range. If multiple scans have been collected, the last scan will be closest to equilibrium and should be chosen for analysis. Earlier scans collected during the approach to equilibrium can be excluded during editing. For multi-wavelength AUC experiments, a spectral decomposition scan file can be loaded as well (using file naming convention 'SSF-runID.auc'). Files without edit profile or of type different than '*Buoyancy*' cannot be loaded. Successfully imported experimental data are structured into separate data sets of individual triples (cell/channel/wavelength) typically containing a single scan of the experiment in the form of concentration vs. radial position (OD/fringes/fluorescence emission vs. cm). A typical concentration curve represents a collection of well-defined and nearly symmetrical peaks, each of which can be characterized in terms of 3 parameters: the peak width (parameterized by σ, or the peak's half-width), the peak's radial position, and the peak's amplitude. Importantly, these parameters provide a basis for calculation of the values of interest, such as the density and the apparent partial specific volume of the solute at the radial position of the peak (according to Eq. 11), and the relative amount of each solute in the mixture. Peak identification, however, is complicated by the noisy nature of the raw data, making the separation of noise signals from physically relevant peaks associated with different solutes particularly challenging. To address these challenges, the experimental data are initially fitted using a non-linear least squares regression technique employing Gaussian distributions as basis functions. Given the characteristic peak shape of the solute signals, linear combinations of Gaussian terms are very well suited to parameterize the experimental data. The scans of interest, the meniscus position, the fitting range of each curve, and the bottom of the cell's position are extracted from the corresponding triple's edit profile. These parameters are required for the solution of Eq. 11. The rotor speed, rotor stretch, and centerpiece geometry are retrieved from the openAUC raw data structure. We experimented with different numbers of basis set functions and peak widths and determined that optimal fitting results, as judged by the best combination of fewest basis functions and the smallest root mean square deviation (RMSD) are typically achieved when the basis sets are comprised of 15 to 25 Gaussian functions with σ-values that best describe a single peak. The process of determining an exact number of these functions for each particular curve has been automated based on the obtained minimum RMSD requirement. The resulting fitting curves smoothen the experimental data and improve the signal-to-noise ratio. To separate relevant peaks from those originating from the remaining noise, a radial interval (a "probe") is defined, which slides along the fitted curve in order to check for the existence of a single principal maximum within that range. The width of the interval is controlled by the user-selectable σ-value, which is initialized by default to 0.015 cm, the half-width of a peak typically observed with AAV particles in a CsCl solution with 1.42 g/ml loading concentration. To decide if larger amplitude peaks are relevant or not, the peak's amplitude is compared to the RMSD of the raw data from the fitted curve. A peak is accepted to be relevant when the ratio of the peak amplitude to RMSD is 4 or greater. This approach proved very effective in eliminating spurious peaks obtained from

noise, as well as larger amplitude peaks which are not physically relevant. When relevant peaks are identified, each peak is approximated with the Gaussian distribution characterized by the peak's position (found with the above mentioned sliding probe algorithm), amplitude (extracted from the fitted curve), and the width as defined by the σ-value. The sigma value for Gaussian basis functions used in the fitting procedure should be adjusted by the user to achieve an optimal overlap with the relevant portion of the fitted curve (see GUI description in "Software implementation" and Fig. 1). The relative concentration (percent of the total) of each peak is computed as the ratio of the volume of the corresponding Gaussian peak and the total volume of the fitted curve. Importantly, the sector-shaped geometry of the centerpiece used in the experiment was taken into account to compute the volume integral of the Gaussian parameterization of the raw data, and the volume integral from a given peak. If the centerpiece has the typical sector shape, contributions of the peaks are expected to monotonously increase when peaks are closer to the bottom of the cell, as the centerpiece's cross-sectional volume increases. In the case of a rectangular channel shape, no such correction is needed. Since the geometry of a centerpiece is derived from the openAUC data set, any type of centerpiece other than the standard sector shape are automatically accounted for in this software.

Software implementation—The '*us_abde*' module provides a convenient user interface to process ABDE experiments. When selecting an openAUC experiment either from the LIMS database or the local disk, all available experiments are screened for openAUC experiments of type '*Buoyancy*' when the user clicks on the '*Load Data*' button. Any selected experiment is checked for the existence of an associated edit profile, which is required for subsequent raw data analysis. If an edit profile cannot be found, the data upload is aborted, and a message is presented to alert the user. Before a data set is loaded, the user has the option to select between automatic fitting of all triples, or manual operation (*'[AUTO] Fit All Triples*' checkbox). When auto-fitting mode is selected, data loading is immediately followed by automatic processing of all triples belonging to the run, (raw data fit, peak identification, calculation of relative peak contributions, see above) based on preset values for the loading concentration, partial specific volume and molar mass of the density forming material. In manual mode, the user can choose to analyze the currently selected triple (by clicking '*Fit Current Triple*' button) and make individual adjustments for the σ-value, density forming gradient material's loading concentration, partial specific volume, and molar mass. Experimental parameters for a loaded experimental data set are divided into 2 groups. The first group includes the meniscus position, rotor stretch, centerpiece bottom, speed-corrected bottom, buffer density, and temperature. These parameters are non-editable and are inferred from the LIMS database records for the associated edit profile (data range, meniscus position, buffer density, centerpiece geometry, and temperature), or computed internally after completion of the data upload (rotor stretch, speed-corrected bottom). The buffer density is calculated by UltraScan based on the concentration and type of buffer components used to dissolve the gradient-forming materials, excluding the gradient-forming material itself. The assumption is made that the concentration of the buffer components is very small compared to the concentration of the gradient-forming material and any changes in the final density distribution due to these components is negligible. The second group of experimental parameters is comprised of the loading density, the density gradient-forming

material's partial specific volume and molar mass, and the peak σ-value. Changing any of these adjustable parameters by the user will trigger the program to automatically re-compute all peak parameters, except the peak position, and update the gradient plot (green line in Fig. 1). A screenshot of the *us_abde* module is shown in Fig. 1. The 'Peak Editor' utility available in this module allows the user to manually define additional peaks that may have been missed by the automated routine ('*Add Peak Manually*' button), or to delete any previously defined peaks ('*Delete Current Peak*' button). These manual manipulations are of great help when the automated peak identification procedure fails to capture all relevant peaks, or mis-identifies non-relevant peaks. These scenarios are possible when more challenging raw data are encountered such as data with unusual noise levels, or for very heterogeneous samples where some relevant peaks may have amplitudes below the pre-defined threshold level. All fitted peak parameters can be accessed from a drop-down list in the main GUI, or can be accessed through the ABDE analysis report by clicking the '*View Report*' button. Importantly, the report is updated automatically each time any manual peak operations described above are performed by the user.

Experimental

Gradient forming material selection and experimental setup—As mentioned above, several density gradient-forming materials are suitable for the measurement of biological macromolecules in ABDE experiments. As an example, we explain here how to use Nycodenz as a gradient material for ABDE experiments, but most considerations apply to other gradient materials as well. Nycodenz is a non-toxic, non-ionic, tri-iodinated derivative of benzoic acid with three aliphatic hydrophilic side chains (Product and information guide for Nycodenz®: http://www.progen.de/media/downloads/datasheets/1002424.pdf). Aqueous solutions of Nycodenz have a very high water activity, and most particles, especially charged particles, will therefore be fully hydrated in solutions of Nycodenz and will band at a low density. Nycodenz is able to form density gradients which cover a density range ideal for measuring a wide range of biological macromolecules. However, due to the high refractive index and strong absorptivity in the UV, Nycodenz and other absorbing, non-ionic gradient-forming materials like metrizamide or iodixanol cannot be used with the UV absorption optics available with the Beckman Proteomelab XLA/I or Optima AUC instruments. For applications with unlabeled molecules absorbing in the UV to be detected with the UV/visible absorption optics, gradient materials like CsCl must be used, which are mostly transparent in the UV. Like Nycodenz and other non-ionic gradient materials, CsCl also has a large refractive index at the concentrations used in ABDE experiments. The shape of the gradient in combination with the strong refractive index will act as a lens and bend any light passing through the ultracentrifuge cell away from the optical path of these detection optics. To mitigate the refractive effects, shorter 3 mm centerpieces should be used to decrease the optical path length, and thereby the refractive effects. When using an absorbing density gradient-forming material, a macromolecule tagged with a fluorescent label that matches the excitation laser can be observed with the Aviv fluorescence detector system (FDS) (MacGregor et al. 2004), which affords additional sensitivity and provides exquisite selectivity for the fluorescently labeled macromolecule. Since the confocal microscope used in the FDS optics is focused to detect only the fluorescent emission of the labeled macromolecule from the top 1–2 mm of the

solution column, any difficulties arising from refraction and UV absorption are avoided. For Rayleigh interference optics, 3 mm centerpieces are also highly recommended to avoid refractive effects from any highly refractive density gradient-forming material. Rotor speeds should be selected between 40 and 60 krpm, with higher speeds providing a larger density range and narrower peaks. Solution columns should take advantage of the entire length of the cell, with menisci at 5.95–6.0 cm to maximize the density range that can be observed. It is also important that the signal from a peak stays within the dynamic range of the detector, and it is important to understand that the signal from the peak increases until equilibrium is reached (see Figs. 2 and 3; for comparison with Fig. 3, the van Holde – Weischet distributions for protein and DNA from a velocity experiment of the same sample are shown in Fig. 4). For UV/visible detection, a maximum peak concentration of 1.0–1.3 OD is recommended, depending on the emission intensity of the wavelength. For the fluorescence detector, the PMT voltage and gain setting should be adjusted to record the maximum peak height below 4000 counts. Proper scaling of the peak signal assures that recordings are linear with respect to concentration and peak integrations are reliable.

Preparation and calibration of Nycodenz standards—According to Eq. 11, the accurate measurement of the loading concentration of the gradient-forming material is an essential prerequisite for the reliability of the gradient-forming material concentration calculation. Only if the density gradient-forming material's loading concentration is accurately known can the precise density be predicted for any position in the gradient. In order to obtain accurate measurements, four standard solutions with known Nycodenz concentrations were prepared and their densities, absorbances and refractive indices were measured. The four Nycodenz standards were prepared by weighing four different amounts of Nycodenz with a Mettler P1210 balance, dissolving each quantity in ddH_2O in a 25 ml volumetric flask, and weighing the resulting solution. All standards were prepared at 23°C. The four standards were determined to have concentrations of 7.28%, 26.52%, 33.52%, and 51.68% (weight/volume). Three orthogonal methods were employed to independently quantify the loading concentration of Nycodenz solutions employed in the ultracentrifugation experiments. Each method was calibrated with the standard Nycodenz solutions to derive the instrument response as a function of concentration. Any one of these methods can be applied to other density gradient-forming materials. However, since CsCl solutions do not absorb at longer UV wavelengths, the photometric approach can only be used at wavelengths < 230 nm for CsCl. For Nycodenz, we collected UV–visible absorbance profiles between 340 and 430 nm. Observations below 1.0 absorbance units between 340 and 430 nm were saved and fitted to a global extinction profile using UltraScan's spectrum fitter module (see (Demeler and Gorbet 2016; Demeler et al. 2022)). A global model with 50 Gaussian terms was fitted to the absorbance data and normalized to a 5% Nycodenz solution (variance of the fit: 1.89×10^{-6}). The fit of these data is shown in Fig. 5, the extinction coefficients for a 5% Nycodenz solution for wavelengths from 340 to 430 nm are presented in SI-1.

Second, we measured density with an Anton-Paar DMA 601 densitometer. The densitometer measurements were taken at 20°C, and the instrument was calibrated with degassed ddH_2O and dried air, taking into account current barometric pressure. Standard solutions were

degassed prior to measurement. Five readings of each solution were taken and averaged; density conversions were calculated with the densitometer module of UltraScan-II (Demeler 2005, 2011). The density calibration could be well fit with a straight line given by Eq. 12:

$$\rho = 3.56 \times 10^{-3} c + 0.998 \tag{12}$$

where c is the Nycodenz concentration in % weight/volume. The line fit is shown in Fig. 6.

Third, a Bausch and Lomb Abbe refractometer was used to record refractive indices of the each stock concentration. The refractometer was calibrated with the internal reference. Based on this calibration, the refractive index of MilliQ-prepared ddH_2O water was measured as 1.330. All refractometer calibration and Nycodenz measurements were taken at 20 °C, and at 589 nm. Each concentration of Nycodenz was measured three times, and the measurements were averaged. The refractive index calibration was fitted to a straight line given by Eq. 13:

$$\mathrm{RI} = 1.55 \times 10^{-3} c + 1.33 \tag{13}$$

The line fit is shown in Fig. 6.

Among the three methods, the refractometer approach is the preferred method. It has minimal sample requirements, and is highly accurate over a wide range of concentrations, is a fast method to determine concentration, and there is no requirement for the gradient material to have a chromophore.

Determination of the partial specific volume of Nycodenz—Additional parameters needed for the solution of Eq. 11 include the molar mass of the density gradient-forming material and the density of the buffer in which the gradient former is dissolved, as well as the partial specific volume of the density gradient-forming material in the buffer in which it is prepared. The buffer density, rotor speed, temperature, meniscus, and bottom of cell positions are determined with UltraScan from the experimental data or reference data in the LIMS database (Stoutjesdyk et al. 2020; Memon et al. 2014). To obtain the partial specific volume of the density gradient-forming material, we employed sedimentation equilibrium experiments. Fixing the known molecular weight of Nycodenz (821 g/mol, (Product and information guide for Nycodenz®: https://www.proteogenix-products.com/documents/pdf/axis-shield/1002424-Nycodenz.pdf) in the fit, the partial specific volume for Nycodenz was allowed to float instead. Three dilutions of a 60% Nycodenz solution were scanned at equilibrium at 20 °C, and at 321 nm and at 329 nm (wavelengths were selected to remain within the dynamic range of the detector) at 40, 50, and 60 krpm using absorbance optics, generating 9 equilibrium profiles. The data were globally fitted with UltraScan-II version 9.9 (Demeler 2005, 2011) to a single species model and a fixed molecular weight distribution model (Demeler 2005). The fixed molecular weight model is degenerate and will fit well to any dataset, generally producing the lowest possible RMSD. The RMSD obtained for the fixed molecular weight model was 7.25×10^{-3}, and for the single species model it was 7.45×10^{-3}. The minimal difference between these RMSD values confirms that the single species model is suitable for these data. A Monte Carlo error analysis (Demeler and Brookes 2008)

of the data determined the partial specific volume of Nycodenz to be 0.4831 ml/g (0.4819, 0.4843). The inverse of the partial specific volume corresponds to a density of 2.070 (2.065, 2.075) g/cm^3, which is in good agreement with the anhydrous density reported for Nycodenz by the manufacturer (2.1 g/cm^3). The equilibrium results for Nycodenz are shown in Fig. 7. For CsCl, we determined a partial specific volume of 0.2661 ml/g.

Analytical buoyant density equilibrium experiments—Bovine thyroglobulin (Sigma-Aldrich, cat no. T1001) and an AAV9 preparation were measured in an Optima AUC (Beckman Coulter, Indianapolis) at the Canadian Center for Hydrodynamics at the University of Lethbridge. The thyroglobulin loading concentration was 0.374 μM (0.125 OD 280 nm/cm), and the AAV9 loading concentration was 0.2 OD 260 nm/cm, with a titer of 6.82×10^{12} vg/ml. The protein was suspended in a CsCl concentration of 1.39 g/ml, and the AAV sample in a 1.40 g/ml concentration. All ABDE samples were loaded with 110 μl volume into 3 mm titanium centerpieces (Nanolytics, Potsdam, Germany). The rotor speed was set to 60,000 rpm and the temperature to 20°C. All data were collected in intensity mode. Time-invariant noise subtraction and conversion from intensity to pseudo-absorbance data were performed with the pseudo-absorbance module in UltraScan-III (Mortezazadeh and Demeler 2023). The thyroglobulin integration results are shown in Fig. 2A, the approach to equilibrium data in Fig. 2B. The integration results for the preparation of AAV9 indicate a series of peaks reflective of multiple loading states (Fig. 3A), their approach to equilibrium is shown in Fig. 3B. The AAV9 sample exhibits significant heterogeneity, but nevertheless, individual loading species present in significant amounts can be well resolved and identified based on their integration results. The heterogeneity in this case is evident from the fact that individual peaks do not reach to baseline, and the heterogeneity forms an elevated baseline, suggesting a broad range of contaminants in the preparation. In Fig. 3A and Fig. 3B, the elevated baseline toward the bottom of the cell, as well as the total sum of the integrated peak area, which only adds up to 57.7% of the total absorbance, indicates that additional species are present, and that they are broadly distributed, supported also by results shown in Fig. 4. Additionally, 224 nm measurements include contributions from CsCl, therefore, a slight CsCl gradient contribution contributes to the baseline offset.

Multi-wavelength sedimentation velocity experiments—The same AAV9 sample that was measured as an ABDE experiment described above was also measured as a sedimentation velocity experiment in Dulbecco's phosphate buffered saline. The experiment was performed at 14,600 rpm by scanning a single 1.2 cm Epon centerpiece cell in intensity mode, measuring 26 wavelengths between 240 and 290 nm in 2 nm increments. The multi-wavelength data were processed by wavelength decomposition as described in Henrickson et al. 2022 to generate a diffusion-corrected integral sedimentation distribution for protein and DNA separately, according to the enhanced van Holde–Weischet method (Demeler and Holde 2004). The results are shown in Fig. 4. Visualizing the protein signal only, all capsid loading states are visible. Empty capsids are only seen in the protein signal around 65 S, partially filled capsids are seen between 65 and 95 S, filled capsids are seen where protein and DNA signals overlay at sedimentation coefficients at and above 95 S. The DNA signal in the velocity experiments shows comparable concentrations of filled and partially filled species, and about 10% of a nucleic acid contaminant sedimenting with sedimentation

coefficients less than 65 S. About 65% of the protein signal migrated with sedimentation coefficients corresponding to filled capsids, 15% with partially filled capsids, and 20% with empty capsids.

Discussion

Significant growth in the viral vector-based gene therapy industry has renewed interest in AUC as a gold-standard method to characterize AAV preparations to quantify and distinguish empty from full capsids. As shown in this work, ABDE experiments are proven to be accurate and offer high precision and high resolution quantification for proteins, DNA and protein/DNA complexes. The apparent partial specific volumes derived from the analysis are consistent for macromolecules of the same kind, as long as the buffer and gradient material are at the same concentrations. However, observed partial specific volumes are highly dependent on the gradient material used. For example, an apparent partial specific volume of 0.8 ml/g for thyroglobulin in a high concentration CsCl solution is higher than the value observed in a dilute aqueous solution, which is closer to 0.73 ml/g. Similarly, anionic DNA exhibits a much lower apparent partial specific volume when dissolved in CsCl compared to non-ionic Nycodenz due to the formation of ionic bonds with dense Cs ions in CsCl. A new peak finder and peak characterization module was added to UltraScan that facilitates quantification and characterization of peaks, providing run-to-run consistency for the determined apparent partial specific volumes and peak identities. The use of intensity data further improves noise characteristics when processing raw experimental data with UltraScan's pseudo-absorbance utility module, and doubles the capacity of the ultracentrifuge by allowing a second sample to be measured in each cell, enhancing throughput (Mortezazadeh and Demeler 2023). The new peak finder software automatically scans and analyzes all datasets in a single run and generates a text file report, which simplifies and speeds up analysis without sacrificing accuracy. The user has the ability to fine-tune density gradient-forming material loading concentrations, molar mass and partial specific volume to choose between different gradient-forming materials for maximum flexibility, and to adjust the peak sigma for maximum overlap with the peak shape. Sedimentation velocity analysis of the AAV9 sample processed with the ABDE method provided complementary validation of the AAV9 sample composition. Taking into account that Fig. 3A was acquired at a single wavelength (224 nm, representing mainly protein signal), there is remarkably good agreement in the relative concentrations detected by both sedimentation velocity and ABDE methods. Together, low sample requirements, high resolution, and precision, as well as rapid analysis with the new peak fitting software in UltraScan suggest that ABDE experiments are accurate, and readily deployed for the reliable quantification and identification of AAV loading species.

Supplementary Material

Refer to Web version on PubMed Central for supplementary material.

Acknowledgements

We thank Viviana Gradinaru and Zhe Qu, California Institute of Technology, for providing the AAV9 sample, and thank Saeed Mortezazadeh, University of Lethbridge for assistance with the pseudo-absorbance module in

UltraScan. We also thank Lauren Tsai and Micah Tatum, The University of Texas Health Science Center San Antonio, for performing the Nycodenz measurements. This work was supported by the Biomolecular Interaction Technology Center, University of Delaware, the Canada 150 Research Chairs program (C150-2017-00015, BD), the Canada Foundation for Innovation (CFI-37589, BD), the National Institutes of Health (1R01GM120600 to EB, AS, BD) and the Canadian Natural Science and Engineering Research Council (DG-RGPIN-2019-05637, BD). The Canadian Natural Science and Engineering Research Council is acknowledged for supporting AH through a scholarship grant.

Data availability

The UltraScan software used to analyze the AUC data is open source and freely available from the Github repository (https://github.com/ehb54/ultrascan3). The AUC data is available in openAUC format upon request from the authors, and is stored in the UltraScan LIMS server at the Canadian Center for Hydrodynamics.

References

Challis RC, Ravindra Kumar S, Chan KY, Challis C, Beadle K, Jang MJ, Kim HM, Rajendran PS, Tompkins JD, Shivkumar K, Deverman BE, Gradinaru V (2019) Systemic AAV vectors for widespread and targeted gene delivery in rodents. Nat Protoc 14(2):379–414. 10.1038/s41596-018-0097-3 [PubMed: 30626963]

Cölfen H, Laue TM, Wohlleben W, Schilling K, Karabudak E, Langhorst BW, Brookes E, Dubbs B, Zollars D, Rocco M, Demeler B (2010) The open AUC project. Eur Biophys J 39(3):347–359. 10.1007/s00249-009-0438-9 [PubMed: 19296095]

Demeler B (2005) UltraScan a comprehensive data analysis software package for analytical ultracentrifugation experiments. In: Scott DJ, Harding SE, Rowe AJ (eds) Modern analytical ultracentrifugation: techniques and methods. Royal Society of Chemistry (UK), p 210–229

Demeler B (2011) UltraScan-II version 9.9, release 1585-a comprehensive data analysis software package for analytical ultracentrifugation experiments. https://github.com/ehb54/ultrascan2

Demeler B, van Holde KE (2004) Sedimentation velocity analysis of highly heterogeneous systems. Anal Biochem 335(2):279–288. 10.1016/j.ab.2004.08.039 [PubMed: 15556567]

Demeler B, Brookes EH (2008) Monte Carlo analysis of sedimentation experiments. Colloid Polym Sci 286:129–137

Demeler B, Gorbet G (2016) Analytical ultracentrifugation data analysis with UltraScan-III. Ch. 8. In: Uchiyama S, Stafford WF, Laue T (eds) Analytical ultracentrifugation: instrumentation, software, and applications. Springer, Japan, pp 119–143

Demeler B, Brookes EH, Gorbet GE, Savelyev A, Zollars D, Dubbs B (2022) UltraScan data analysis software for analytical ultracentrifugation experiments and hydrodynamic modeling. https://github.com/ehb54/ultrascan3

Deng S, Oka K (2020) Adeno-associated virus as gene delivery vehicle into the retina. Methods Mol Biol 2092:77–90 [PubMed: 31786783]

Green AA, Hersam MC (2011) Nearly single-chirality single-walled carbon nanotubes produced via orthogonal iterative density gradient ultracentrifugation. Adv Mater 23(19):2185–2190. 10.1002/adma.201100034 [PubMed: 21472798]

Henrickson A, Gorbet GE, Savelyev A, Kim M, Hargreaves J, Schultz SK, Kothe U, Demeler B (2022) Multi-wavelength analytical ultracentrifugation of biopolymer mixtures and interactions. Anal Biochem 652:114728. 10.1016/j.ab.2022.114728 [PubMed: 35609686]

MacGregor IK, Anderson AL, Laue TM (2004) Fluorescence detection for the XLI analytical ultracentrifuge. Biophys Chem 108:165–185 [PubMed: 15043928]

Memon S, Riedel M, Janetzko F, Demeler B, Gorbet G, Marru S, Grimshaw A, Gunathilake L, Singh R, AttigLippert NT (2014) Advancements of the UltraScan scientific gateway for open standards-based cyberinfrastructures. Concurr Comput Pract Exper. 10.1002/cpe.3251

Meselson M, Stahl FW (1958) The replication of DNA in *Escherichia coli*. Proc Natl Acad Sci 44:671–682 [PubMed: 16590258]

Mortezazadeh S, Demeler B (2023) Systematic noise removal from analytical ultracentrifugation data with UltraScan. Eur Biophys J. 10.1007/s00249-023-01631-6

Sambrook J, Fritsch ER, Maniatis T (1989) Molecular cloning: a Laboratory Manual, 2nd edn. Cold Spring Harbor Laboratory Press, Cold Spring Harbor, NY

Stoutjesdyk M, Henrickson A, Minors G, Demeler B (2020) A calibration disk for the correction of radial errors from chromatic aberration and rotor stretch in the Optima AUC™ analytical ultracentrifuge. Eur Biophys J 49(8):701–709. 10.1007/s00249-020-01434-z [PubMed: 32388675]

The Axis-Shield Product information guide for Nycodenz®. https://www.proteogenix-products.com/documents/pdf/axis-shield/1002424-Nycodenz.pdf

Wang S, Guo Y, Pu WT (2021) AAV gene transfer to the heart. Methods Mol Biol 2158:269–280. 10.1007/978-1-0716-0668-1_20 [PubMed: 32857380]

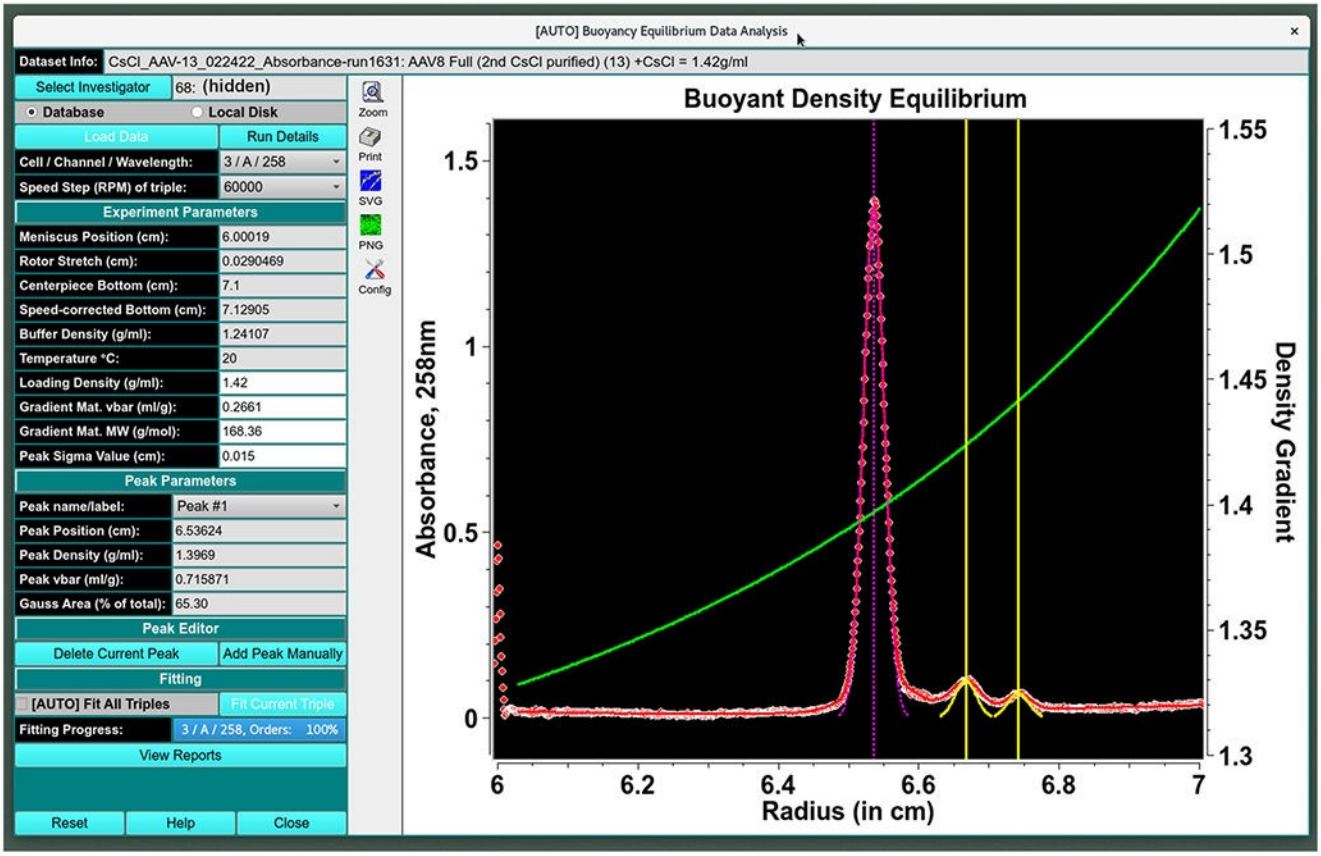

Fig. 1.

GUI of the us_buoyancy_auto module. Raw data and fitted curve are depicted in red. Gaussian functions and their positions associated with identified relevant peaks are shown in yellow; the currently selected peak and its position is shown in purple for clarity. The density gradient is plotted in green, and is linked to the right y-axis, showing g/ml

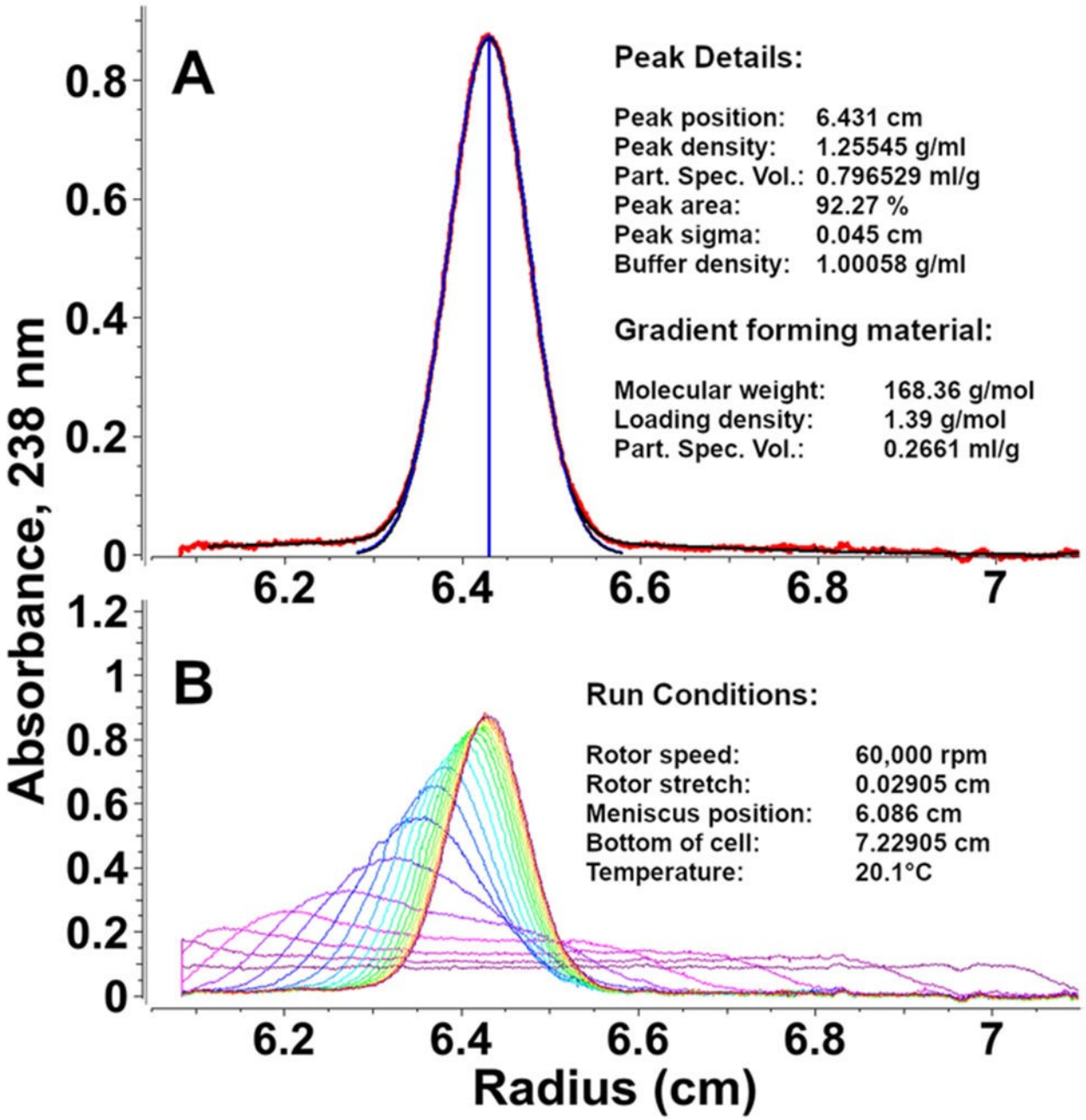

Fig. 2.

Peak integration of thyroglobulin in a CsCl density gradient. **A** Integration plot of the last scan of the ABDE experiment shown in **(B)**, which was taken at equilibrium. The Gaussian fit and peak center are shown in blue, the raw data is shown in red, and the raw data fit is shown in black. **B** Approach to equilibrium of an ABDE experiment of thyroglobulin in a 1.39 g/ml CsCl density gradient. The time variable is shown as a rainbow color gradient, starting at purple and ending at red. As can be seen from the initial scan, the protein floats up from the bottom of the cell and sediments from the meniscus side. The initial scan has an

absorbance of less than 0.1 OD, but the equilibrium concentration at the center of the peak is 0.9 OD

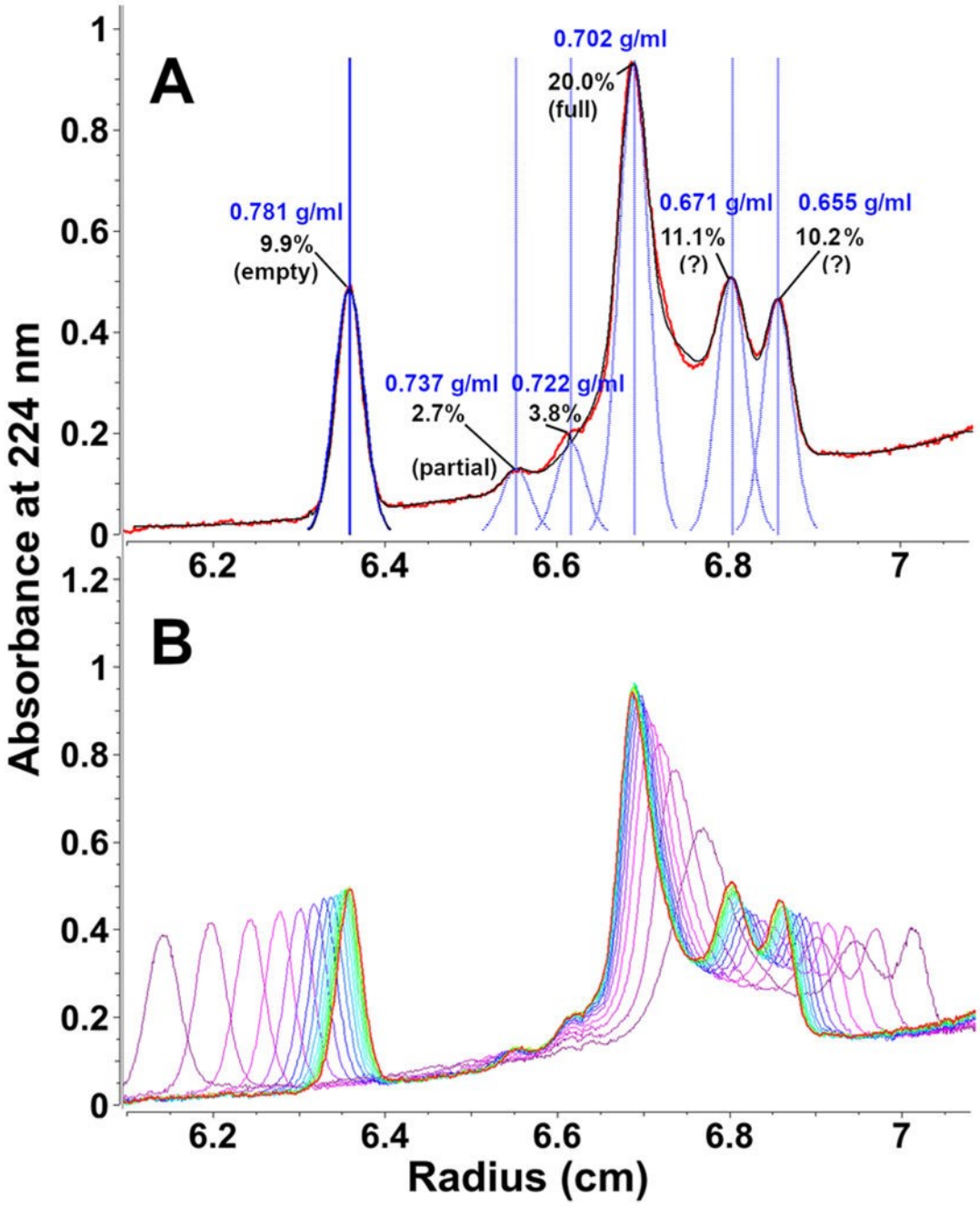

Fig. 3.

AAV9 preparation, containing varying loading states, separated in a CsCl ABDE experiment measured at 224 nm with UV intensity mode. **A** Peak integration of the last scan (at equilibrium) performed with UltraScan, finding 6 different peaks with relative amounts indicated in black text, and apparent partial specific volumes in blue text. The integration sigma value was set to 0.017 cm. **B** Approach to equilibrium of the AAV preparation

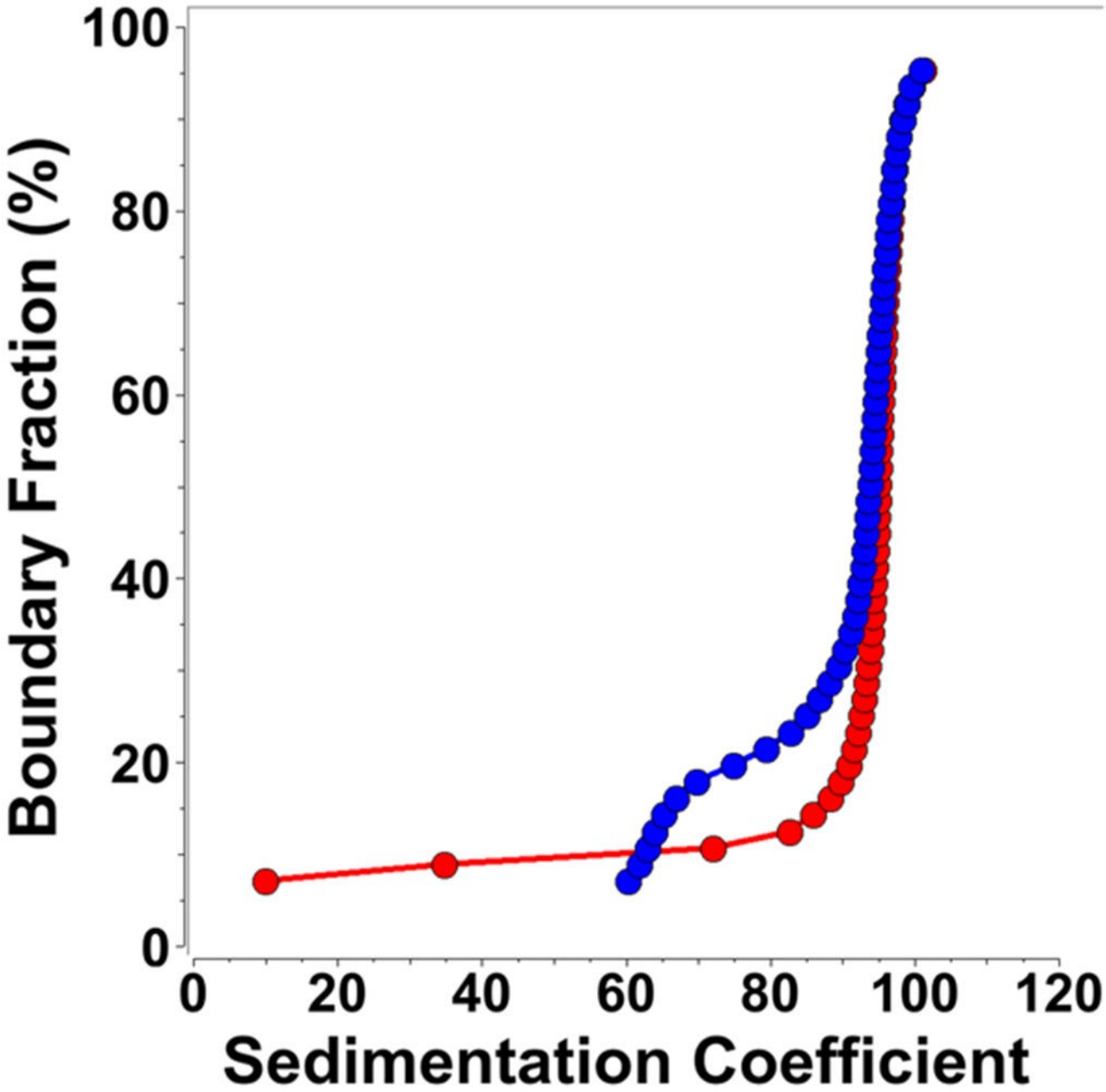

Fig. 4.

Diffusion corrected integral sedimentation coefficient distributions from the multi-wavelength AUC velocity data of the same AAV9 sample shown in Fig. 3A for comparison with the ABDE experimental data. The multi-wavelength data are decomposed into the protein signal (blue) and the DNA signal (red)

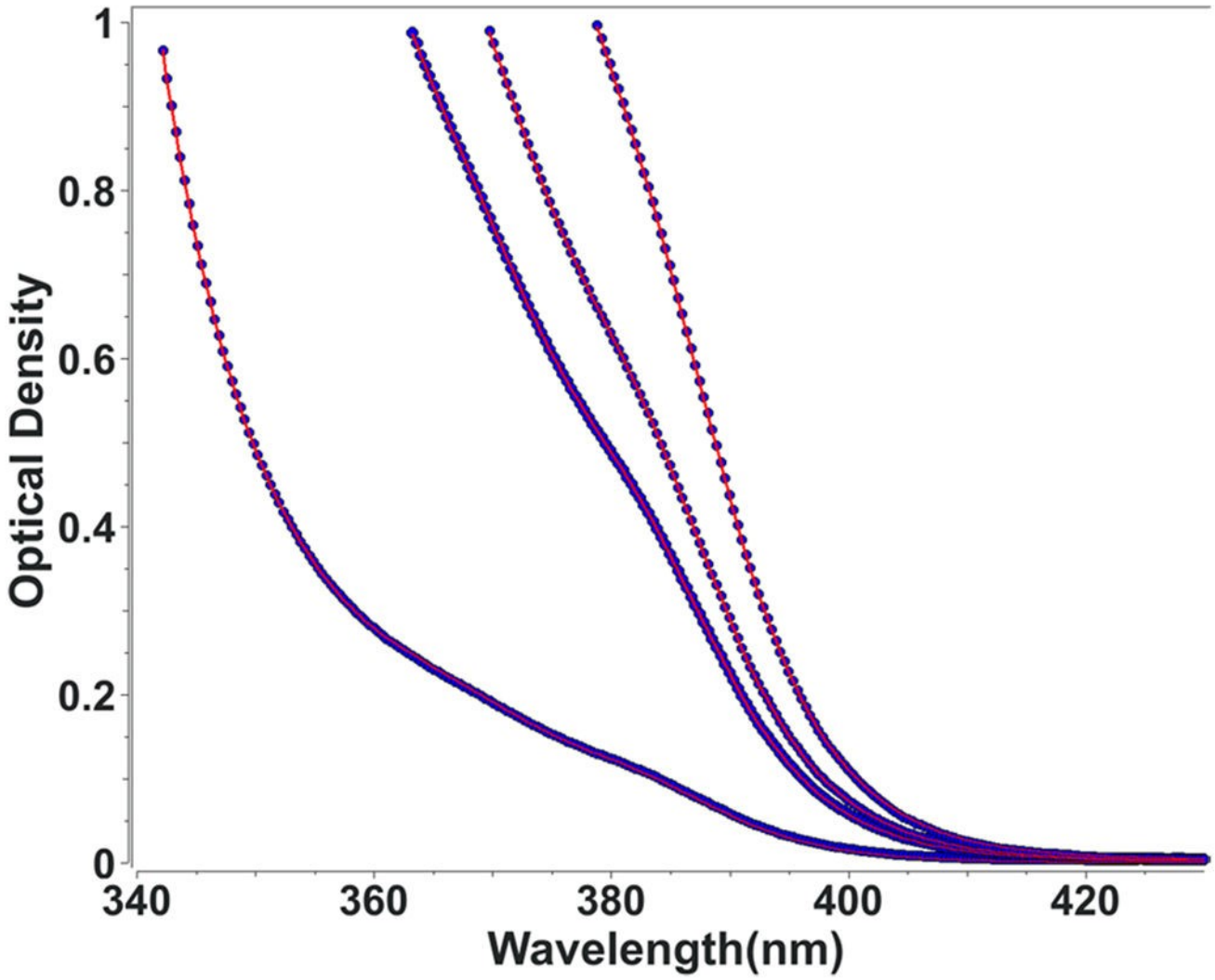

Fig. 5.

Absorbance scans of four Nycodenz concentration standards (blue circles), and their global extinction fit (red lines) to 50 Gaussian terms as determined with UltraScan (see references (Demeler and Gorbet 2016; Demeler et al. 2022) for details). Only values below 1.0 OD were included in the fit. The global model was normalized for a 5% Nycodenz solution, the extinction coefficients over this wavelength range are provided in Supplemental Information SI-1

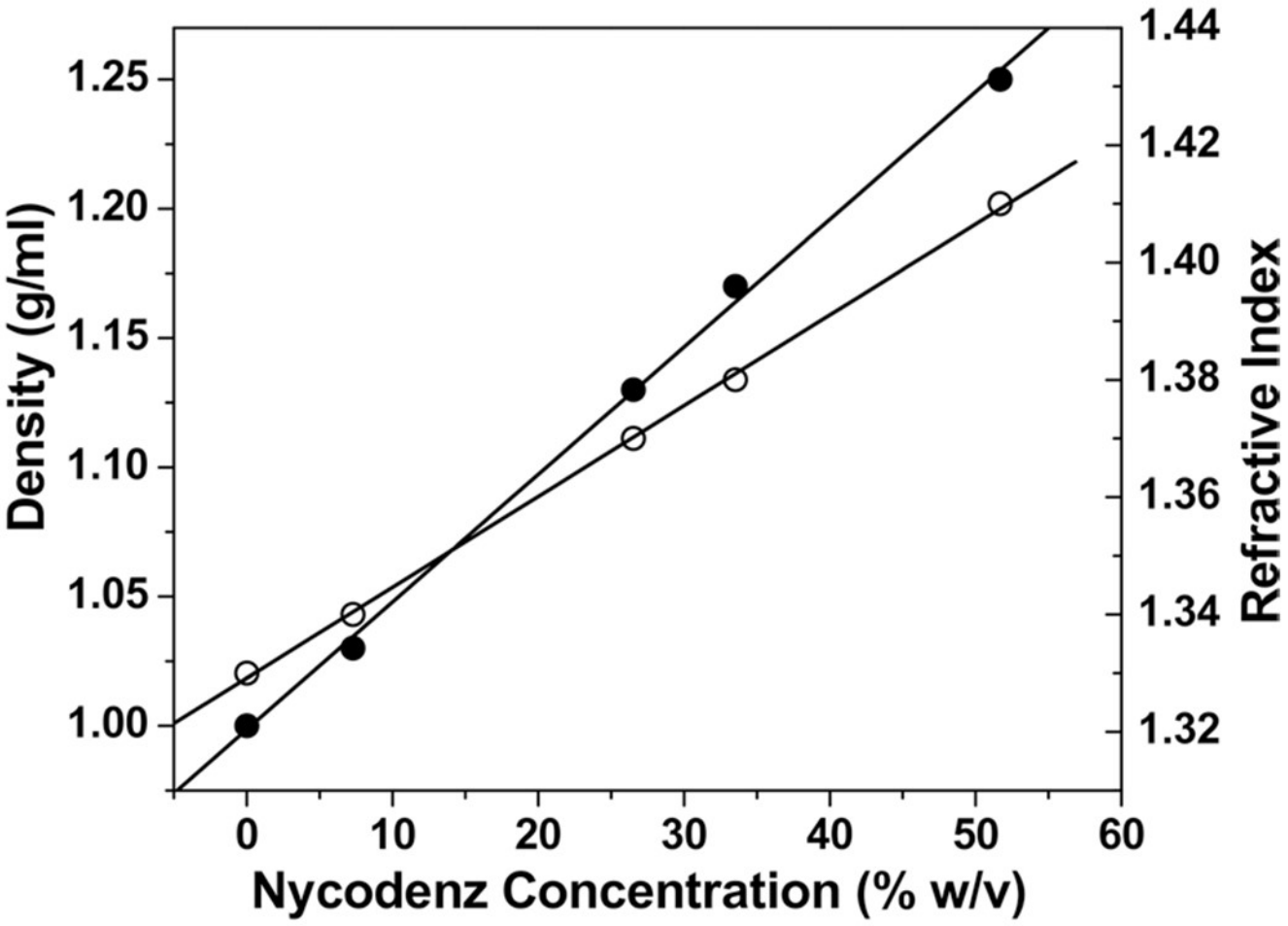

Fig. 6.

Calibration of Nycodenz concentration measurements. Four Nycodenz concentration standards were measured by densitometry (filled circles) and refractive index (open circles). All measurements were fitted well by straight lines, with known values for ddH_2O water included in the fit. See “Methods and results” section for line equations

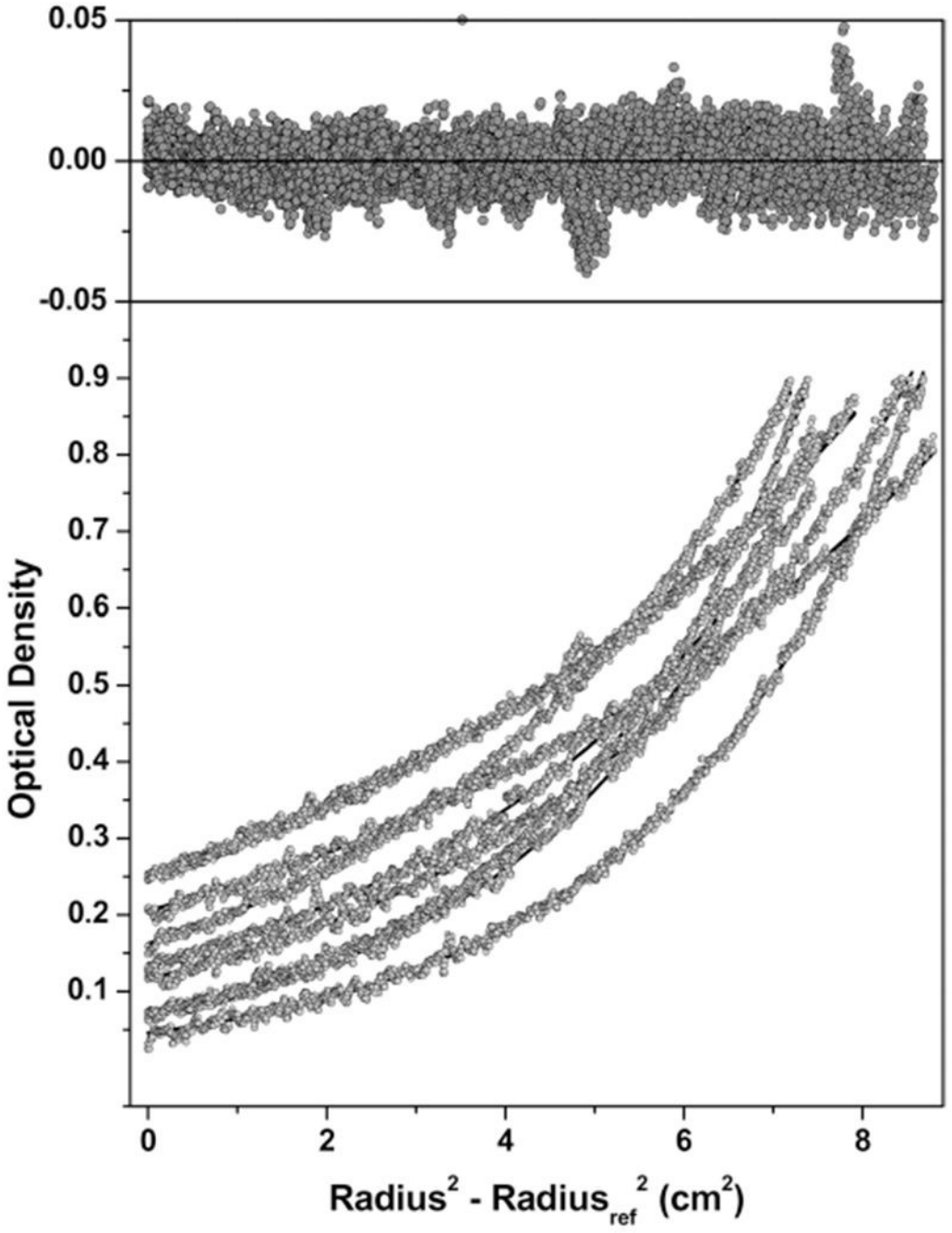

Fig. 7.

Sedimentation equilibrium data for Nycodenz. Scans were taken at 40, 50, and 60 krpm for 3 loading concentrations, generating 9 datasets that were globally fitted, holding the known molar mass constant. Experimental data are shown as gray circles, solid lines represent the fit to a single species model. Upper panel shows random residuals throughout the entire concentration range